Research Article

Journal of Environmental Nanotechnology

Preparation and Characterization of Nanocrystalline Strontium - Doped $SmAlO_3$ Fast Oxide Conductors

N. Kalaivani, M. Rajasekhar*

Department of Chemistry, Government Arts College, Dharmapuri, TN, India

Received: 08.10.2018 Accepted: 02.12.2018 Published: 30-06-2018

*drmrchem@gmail.com

ABSTRACT

$Sm_{1-x}Sr_xAlO_3$ ($0 \leq x \leq 0.5$) powders synthesize with the use of Samarium nitrate, Strontium nitrate, Aluminum nitrate and aspartic acid (fuel) by assisted combustion method, and it heats at 550˚C for 6 hours. The thermal decomposition, phase identification, surface morphology and ionic conductivity of the samples study with Thermal gravimetric Analysis./ Differential Thermal Analysis., X-ray diffraction, Scanning Electron Microscopy and four-probe D.C. method, respectively. The formation of $Sm_{1-x}Sr_xAlO_3$ confirms with the use of Fourier Transformer Infra-red studies. The weight gain and loss performance confirm with the use of thermochemical techniques. The nanoparticle size measure with High-Resolution Transmission Electron Microscope studies. The synthesised materials show reasonable ionic conductivity. These results indicate the assisted combustion method is a promising method to prepare nanocrystalline $Sm_{1-x}Sr_xAlO_3$ for the solid oxide fuel cell.

Keywords: High-Resolution Transmission Electron Microscope; Ionic conductivity; Scanning Electron Microscopy; Thermal analysis.

1. INTRODUCTION

The electrolyte with high oxygen ion conductivity is a key component and wide range of potential applications with including the electrolyte as oxygen sensors in solid oxide fuel cells and acting as an oxygen-permeable membrane in catalytic systems. (Stuart A. Hayward and Simon A. T. Redfern, 2004; Fang *et al.* 2004). Although the research into fast oxide conductors can be traced back to the study of fluorine ion conduction in lead fluoride by Faraday (1839), commercial application high-temperature solid oxide fuel cells which offers a clean, more efficient energy conventional power plant, pollution-free technology to electrochemically generate electricity at high efficiencies, the bottoming cycle of an electronic power plant, domestic water heater and power units, high power density along with a small physical size, high volumetric power density and electric vehicle can be achieved by improving the material properties used for the components (John B. Goodenongh and Yun-Hui Huang, 2007; Young-Hag Koh *et al.* 2006).

Solid Oxide Fuel Cell is highly promising energy conversion devices to improve energy efficiency to provide society with clean energy-producing technology, low pollution output and great fuel flexibility. The high temperature of operation (800-1000˚C) enable the solid oxide fuel cell to operate with existing fossil fuels to give very high-efficiency conversion of fuels to electricity and efficiently coupled with gas turbines. SOFCs quiet and non-polluting, and their inherent high efficiency leads to lower greenhouse gas emissions. (Steele and Heinzel, 2001).

The study uses an aided combustion method to synthesise Nd_2Mo_2-$xGaxO_9$ Nano powders with various molar ratios. The size and shape of the Nd2Mo2-xGaxO9 synthesised product were studied on phase evaluation. Because of the possible uses in solid oxide fuel cells, oxygen sensors, oxygen pumps, and oxygen-permeable membrane catalysts, oxide materials with high oxygen ion mobility are receiving a lot of interest.

2. EXPERIMENTAL AND CHARACTERIZATION PROCESSES

The nanocrystalline$Sm_{1-x}Sr_xAlO_3$powder was synthesized by assisted combustion method with high purity $Sm(NO_3)_3$ (Sigma Aldrich, >99.9%), $Sr(NO_3)_2$ (Sigma Aldrich, >99.9%), $Al(NO_3)_3$ (Sigma Aldrich, >99.9%) and aspartic acid (Sigma Aldrich, >99.9%) as fuel. To achieve a homogenous solution, all of the reagents were dissolved in double-distilled deionized water in the required stoichiometric proportions of the starting ingredients.

This solution was kept at constant heating at 80˚C to obtain the foamy powders of $Sm_{1-x}Sr_xAlO_3$and the foamy powder was carried out in a muffle furnace at 550˚C for six hours.

3. STRUCTURAL CHARACTERIZATION ANALYSIS

X-ray powder diffraction (XRD) data were collected at room temperature with a diffractometer (Model: Philips X` Pert MPH^{R}) with Cu Kα radiation. The data were recorded in the 2θ range of 10-70˚ with a 0.02˚ steps. The particle size and morphology of the produced powder were analysed with a JEOL scanning electron microscopy SEM (Model: JSM-840A) equipment with INCA was used to determine the morphology of samples.

The thermal decomposition of the polymeric precursors was characterized by Perkin-Elmer TG/DTA thermal analysis (Model; Pyris Diamond). The TGA is a process that relies on measuring the change in physical and chemical properties of a sample as a function of temperature (with constant heating rate) or as a function of time (with constant temperature). It is predominantly used for determining the features of a material that exhibit either mass loss or gain due to decomposition, oxidation or loss of volatiles. Differential thermal analysis is a technique in which the temperature of a sample is compared with that of inert reference material during the programmed change of temperature.

The particle size of the synthesized powder was observed by means of a JOEL transmission electron microscopy (Model: 1200 EX). The synthesized powder was analysed with FTIR spectrometry. (Agilent Cary 630 FTIR spectrometer) in which region of about 4000-400 cm^{-1}. The ionic conductivity of the sintered pellets was measured by a dc-four probe method in which temperatures range 200-700 ^{0}C in air.

4. RESUT & DISCUSSION

4.1 Analysis of Crystal Structure

The x-ray diffraction pattern of $Sm_{1-x}Sr_xAlO_3$($0 \leq x \leq 0.5$) samples are shown in Fig. 4. 1. All the samples indicated single-phase materials and the pattern indexed on the basis of the orthorhombic perovskite structure (space group: Pbnm). The sample calcined at 550°C for 6 h exhibits a single phase without any impurities. The data concluded that the lattice volume increased with increasing Sr content x. These results strongly suggested that assisted combustion method required much lower calcination energy with a shorter time duration than the solid-state reaction method.

The average crystallite size of the sample was calculated by using the Scherrer equation.

$$D=0.9\lambda/\beta \cos \theta$$

Where D is the crystallite size in nm, λ is the radiation wavelength (for Cu Kα radiation=1.54 A˚), β is the broadening of the line (half-width) in radians and θ is the diffracting peak angle. The average crystallite size of $Sm_{1-x}Sr_xAlO_3$nano powder is at various compositions. The particle size measured from XRD data. The smaller average crystallite size (nanoparticle) has been achieved by using assisted combustion method compared to the conventional solid-state reaction method and other methods.

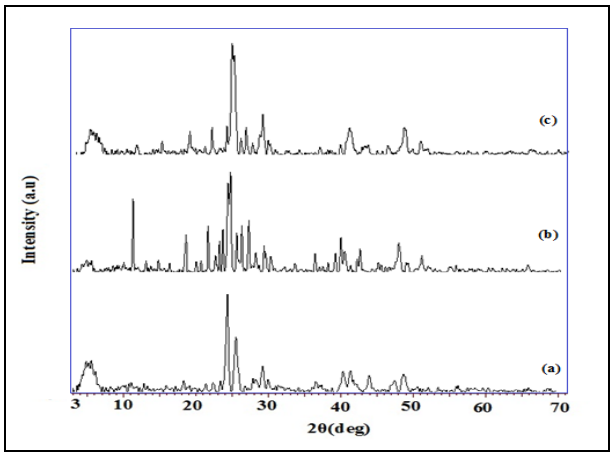

Fig 4.1: X-ray diffraction pattern of $Sm_{1-x}Sr_xAlO_3$

4.2 Scanning Electron Microscopy

Fig. 4.2. Shows SEM analysis of $Sm_{1-x}Sr_xAlO_3$ nanopowder. The materials prepared by assisted combustion method using aspartic acid showed a spongy aspect, and the particles linked together in agglomerates of different sizes and shapes. The loose and porous structure of these materials can be attributed to a significant gas evolution during the combustion reaction (Bansal and Zhong, 2006; Berger *et al.* 2007). Substantial particle growth was observed upon sintering for 6 h at 823 K., but the structure remained highly porous, which resembled the typical cathode structure for SOFC. However, Gallium doping significantly improves grain growth. The doped samples have a 2 μm grain size on average. The crystallites were 24 nm in size on average. Particles aren't spread evenly. The manufactured goods' particles are nanoscale in size.

4.3. Thermal Analysis (TGA/DTA)

$Sm_{1-x}Sr_xAlO_3$nano crystalline powder has been studied before calcination with thermogravimetric analysis (TGA) in the air is shown in Fig. 4.3. Fig 4.3. Showed that thermal decomposition was completed at 700–750 °C. The first decomposition stage up to 250°C can be assigned to the loss of adsorbed water1 (Da Corte and Da Conceicao, 2013), the second stage at about 350–450 °C can be associated with the decomposition of combustion residues that are not burnt during the fast combustion reaction and the third stage at about 500°C can be observed the dissociation of carbonates during the combustion and starting of the formation of

$Sm_{0.5}Sr_{0.5}AlO_3$ phase. Fig.4.3 shows the corresponding DTA curve for the synthesized powders. For the samples prepared by this method with aspartic acid, endothermic peaks are observed with more intense at 550 °C, which indicated the decomposition of organic residues (Ghosh *et al.* 2005).

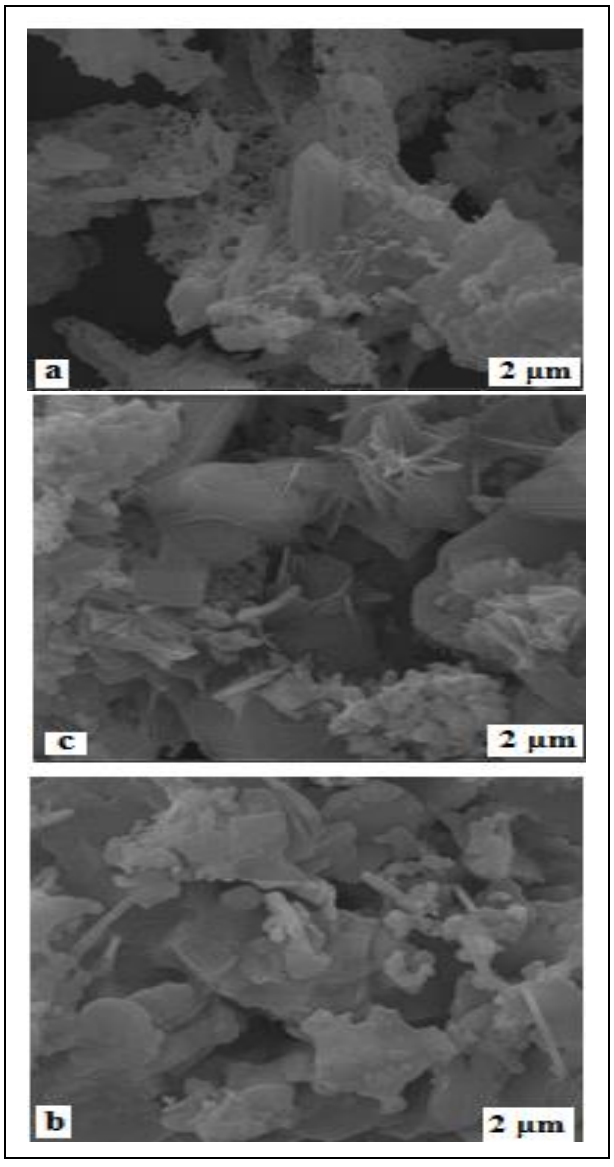

Fig 4.2: SEM photograph of $Sm_{1-x}Sr_xAlO_3$

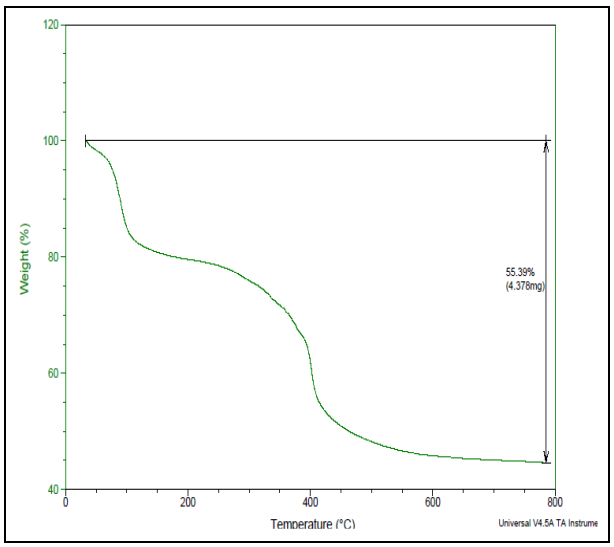

Fig. 4.3: TGA &DTA of $Sm_{0.5}Sr_{0.5}AlO_3$

4.4 FTIR Analysis

FTIR spectroscopy was used to confirm the functional groups present in the crystal and is investigated their vibrational behaviour in the solid-state of $Sm_{1-x}Sr_xAlO_3$ powder; it was recorded in the range of 4000 cm^{-1} to 400cm^{-1}. The infrared spectrums of synthesized samples of $Sm_{0.5}Sr_{0.5}AlO_3$ powder are shown in fig.4.4. The vibration mode of chemically linked hydroxyl groups may be ascribed to the broadband at 1472.0 cm^{-1}. The broadband at 1472.0 cm^{-1} can be attributed to the vibration mode of chemically linked hydroxyl groups. The signal at 819.1 cm^{-1} corresponds to the H-O-H bond mode, indicating that moisture was present in the sample. The peak that appeared at 1410.9 cm^{-1} is due to the presence of CO_2 in the sample. The sample $Sm_{0.5}Sr_{0.5}AlO_3$exhibited a low-intensity peak at 754.5 $cm^{-1,}$ and the sample exhibited three peaks obtained between the wavelength regions 800-1000 cm^{-1} and observed at 891.1, 1091.1 cm^{-1}. The peak that appeared at 1541.8 cm^{-1} is related to the O-H stretching vibration of H_2O in the sample. The broadband at 1472.8 cm^{-1} can be assigned to the vibration mode of chemically bonded hydroxyl groups.

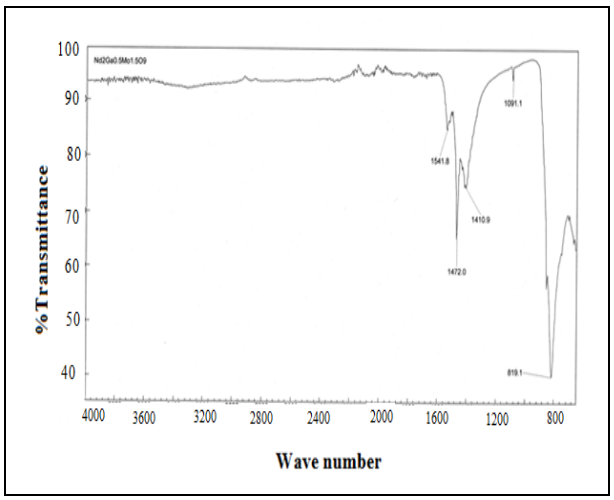

Fig. 4.4: FT-IR spectrum of $Sm_{0.5}Sr_{0.5}AlO_3$

4.6 Conductivity Studies

The Arrhenius plot of conductivity of the $Sm_{1-x}Sr_xAlO_3$samples is shown in Fig 4.5.

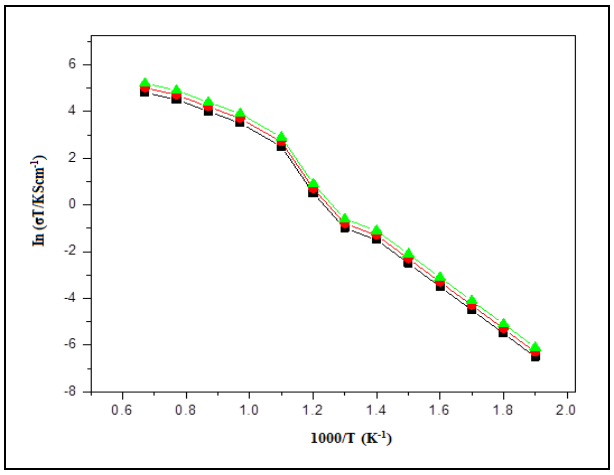

Fig. 4.5: Arrhenius plot for overall conductivity for $Sm_{1-x}Sr_xAlO_3$ sample.

For pure $SmAlO_3$, a dramatic change of conductivity occurs at around 566˚C and is due to a phase transition. The Sr-doped $SmAlO_3$ samples exhibit slightly improved conductivity at lower and higher temperatures. Generally, the higher unit - cell free volume in the oxide ion conductor is easier for oxygen-ion diffusion. On Sr – doping, the cell parameter is decreased. Thus, the substitution of Sr greatly increases the free volume, and therefore the ionic conductivity of Sr-doped samples also increases remarkably. It can also be seen that sharp conduction increases up to x=0.5 in $Sm_{1-x}Sr_xAlO_3$. The $Sm_{1-x}Sr_xAlO_3$sample exhibits the conductivity of 0.166 S cm^{-1} at 800°C, it compared with 0.12 S cm^{-1} for the undoped$SmAlO_3$. This result confirmed that Al-doping could improve the oxide ion conductivity of $SmAlO_3$ at low and high temperatures. Moreover, the high purity and phase homogeneity of the present sample could help to improve the conductivity of Al-doped $SmAlO_3$ samples.

5. ONCLUSION

The purpose of this study was to use the synthesis approach to improve the performance of $Sm_{1-x}Sr_xAlO_3$. The electrochemical behaviour of $Sm_{1-x}Sr_xAlO_3$-based materials is determined by the synthesis technique and the sintering temperature. The current research was primarily concerned with synthesis and ionic conductivity $Sm_{1-x}Sr_xAlO_3$.

FUNDING

This research received no specific grant from any funding agency in the public, commercial, or not-for-profit sectors.

CONFLICTS OF INTEREST

The authors declare that there is no conflict of interest.

REERENCES

Bansal, N. P. and Zhong, Z., Combustion synthesis of Sm0.5Sr0.5CoO3−x and La0.6Sr0.4CoO3−x nanopowders for solid oxide fuel cell cathodes, J. Power Sources, 158, 148–153(2006). https://doi.org/10.1016/j.jpowsour.2005.09.057

Berger, D., Matei, C., Papa, F., Macovei, D., Fruth, V. and Delorme, J. P., Pure and doped lanthanum manganites obtained by combustion method, J. Eur. Ceram. Soc. 27, 4395–4398(2007). https://doi.org/10.1016/j.jeurceramsoc.2007.02.164

Da Corte, R. V., Da Conceicao, L. and Souza, M. M. V. M., Structural and electrical properties of La0.7Sr0.3Co0.5Fe0.5O3 powders synthesized by solid-state reaction, Ceram. Int. 39, 7975–7982(2013). https://doi.org/10.1016/j.ceramint.2013.03.063

Fang, Q, F., Wang, X. P., Li., Z. S., Zhang, G. G. and Yi, Z. G., Relaxation peaks associated with the oxygen-ion diffusion in $La_{2-x}Bi_xMo_2O_9$ oxide ion conductors, Material science and Engineering A, 370, 365-369(2004). https://doi.org/10.1016/j.msea.2003.02.004

Ghosh, A., Sahu, A. K., Gulnar, A. K. and Suri, A. K., Synthesis and characterization of lanthanum strontium manganite, Scr. Mater., 52, 1305–1309(2005). https://doi.org/10.1016/j.scriptamat.2005.02.020

John B. Goodenough, Yun-Hui Huang, Alternative anode materials for solid oxide fuel cells, Journal of power source, 173, 1-10(2007). https://doi.org/10.1016/j.jpowsour.2007.08.011

Steele, B.C.H. and Heinzel, A., Materials for fuel-cell technologies, Nature, 414, 345-352(2001). https://doi.org/10.1038/35104620

Stuart A Hayward and Simon A T Redfern, Thermodynamic nature of and spontaneous strain below the cubic–monoclinic phase transition in $La_2Mo_2O_9$, J. Phys., Condens. Matte, 16, 3571–3583(2004). https://doi.org/10.1088/0953-8984/16/21/007

Young-Hag Koh, Jong-Jae Sun, Won-Young Choi, Hyoun-Ee Kim, Design and fabrication of three-dimensional solid oxide fuel cells, Journal of power sources, 161, 1023-1029(2006). https://doi.org/10.1016/j.jpowsour.2006.05.043